

# Iterative Compositional Data Generation for Robot Control

Anh-Quan Pham<sup>1\*</sup> Marcel Hussing<sup>1</sup> Shubhankar P. Patankar<sup>1</sup>  
 Dani S. Bassett<sup>1</sup> Jorge Mendez-Mendez<sup>2</sup> Eric Eaton<sup>1</sup>

<sup>1</sup> University of Pennsylvania <sup>2</sup> Stony Brook University

## Abstract

Collecting robotic manipulation data is expensive, making it impractical to acquire demonstrations for the combinatorially large space of tasks that arise in multi-object, multi-robot, and multi-environment settings. While recent generative models can synthesize useful data for individual tasks, they do not exploit the compositional structure of robotic domains and struggle to generalize to unseen task combinations. We propose a semantic compositional diffusion transformer that factorizes transitions into robot-, object-, obstacle-, and objective-specific components and learns their interactions through attention. Once trained on a limited subset of tasks, we show that our model can zero-shot generate high-quality transitions from which we can learn control policies for unseen task combinations. Then, we introduce an iterative self-improvement procedure in which synthetic data is validated via offline reinforcement learning and incorporated into subsequent training rounds. Our approach substantially improves zero-shot performance over monolithic and hard-coded compositional baselines, ultimately solving nearly all held-out tasks and demonstrating the emergence of meaningful compositional structure in the learned representations.

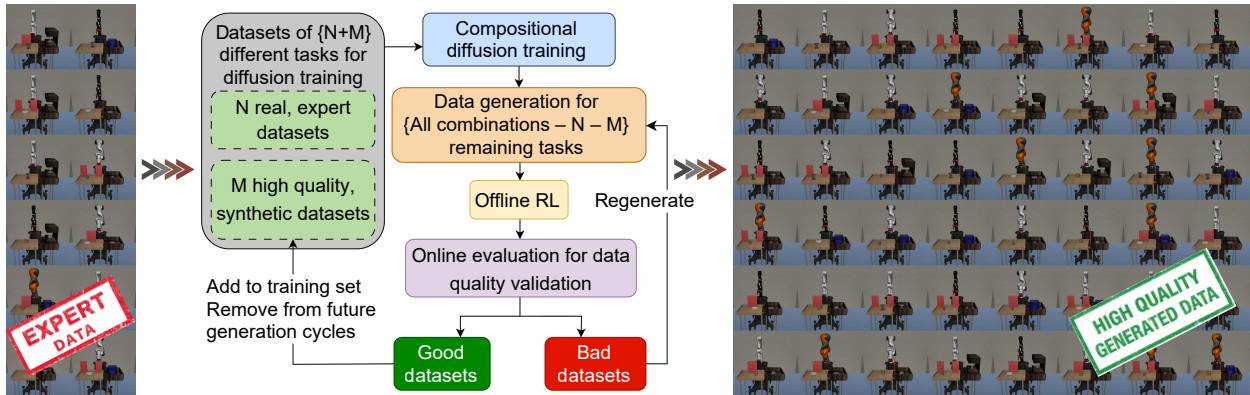


Figure 1: Iterative Compositional Data Generation.

## 1 Introduction

Augmenting model training with self-generated data is a promising approach to improve sample efficiency in domains where collecting real data is expensive. In the context of robotic manipulation, gathering new experience requires operating a physical robot—a process that is labor- and time-intensive, and incurs wear, maintenance, and energy costs. Consequently, collecting data from scratch for every possible new manipulation task quickly becomes impractical as evidenced by various large-scale data collection efforts (Walke

\*Corresponding author: quanpham@seas.upenn.edu

Implementations available at: <https://github.com/anhquanpham/iterative-comp-rl-generation>

---

et al., 2023; O’Neill et al., 2024; Khazatsky et al., 2024). Recent work has shown that current generative models can produce data of sufficient quality to enable training models with substantially reduced real-world experience, including in control settings (Yu et al., 2023; Lu et al., 2023; Liang et al., 2023). However, most existing approaches focus on improving sample efficiency within a single task, and do not leverage self-generated data to accelerate learning on entirely new tasks (Janner et al., 2022; Lu et al., 2023).

In this work, we investigate whether a robot learning system can iteratively improve its ability to solve unseen tasks by generating artificial training data for those unseen tasks with a self-improving generative model (Figure 1). We leverage the insight that cross-embodiment robotic manipulation domains exhibit an inherent compositional structure, whereby each task solution involves a unique composition of reusable models of objects, skills, and controllers. Our central hypothesis is that constructing model architectures that explicitly exploit this compositionality enables *zero-shot generation of high-quality synthetic training data* for novel task compositions, mitigating the need to relearn every task from scratch on a physical robot.

We focus on a reinforcement learning (RL) setting in which tasks are defined compositionally (Mendez et al., 2022a; Hussing et al., 2024), constructed by combining a small number of elements such as robots, objects, obstacles, and goals. Intuitively, machine learning approaches can exploit the inherent combinatorial structure of these domains to generalize to unseen task configurations. Yet, standard single-and multi-task agents require vast amounts of data in such settings, struggling to exploit the compositional structure when the available data is small. Learners are better able to exploit the structure when the policy architecture mirrors the underlying task factorization (Devin et al., 2017; Andreas et al., 2017; Mendez et al., 2022a;b).

One outstanding challenge is that pre-defining such architectures requires strong prior knowledge about the correct decomposition. While much prior engineering knowledge is available for the robotics tasks we consider, it is unclear that these priors are optimal. In this work, we instead train a transformer to learn the compositional structure directly from data, leveraging the transformer interpretation as a graph neural network (GNN). Instead of training a policy on a subset of task combinations and evaluating its zero-shot capabilities, we train a diffusion transformer on the same subset of tasks to *generate training data* for the policies of unseen task combinations, thereby reducing the amount of data required to learn novel behaviors. The model learns a separate tokenizer for each individual task module (e.g., a specific robot, object, or environment) and uses cross-attention to infer the graph that connects these encoders. This yields a representation that is analogous to the hard-coded compositional network used in earlier work (Mendez et al., 2022a), but the structure is learned from data rather than specified a priori.

We first demonstrate that our task-conditional diffusion transformer enables superior zero-shot generalization capabilities compared to monolithic architectures. We then highlight the need for compositional tokenization by showing that models with factor-specific tokenizers achieve improved zero-shot performance relative to models that rely on a single shared tokenizer. Next, we show that models that properly learn the underlying task decomposition can be iteratively trained on their own generated data for unseen tasks to produce training data for solving *more* new tasks without requiring additional real data. Finally, we analyze the learned representations and find that the model discovers a decomposition that differs from previous work, indicating that effective compositional structure can emerge automatically from data.

## 2 Preliminaries

We formulate our problem as generating data of and learning policies in a Markov decision process (MDP)  $\mathcal{M}_n = (S_n, A_n, R_n, \mathcal{P}_n, T)$  where  $S_n$  is the state space,  $A_n$  is the action space,  $R_n$  is the reward function mapping state-action pairs  $(s, a)$  to a scalar  $r$ ,  $\mathcal{P}_n$  is the transition probability function determining the next state  $s'$  given the current state-action pair  $(s, a)$ , and  $T$  is the task horizon. The rewards are bounded to the range  $r \in [0, 1]$ . We say a agent succeeds if, at any state in a trajectory, it achieves the maximum reward of  $r = 1$ . We also define the function  $D_n : S_n \mapsto A_n$  which outputs a termination signal  $d$  that indicates if the agent has moved to an absorbing, non-rewarding state. We consider a set of  $N$  such MDPs  $\{\mathcal{M}_n\}_{n=0}^{N-1}$  and our goal is to learn a policy  $\pi^* = \{\pi_n^*\}_{n=0}^{N-1}$  that maximizes the average probability of success over this set, that is,  $\pi^* \in \arg \max_{\pi} \frac{1}{N} \sum_{n=0}^{N-1} \mathbb{E}_{\pi_n, \mathcal{M}_n} [\mathbf{1}[\max_{0 \leq t \leq T} r_t = 1]]$ .

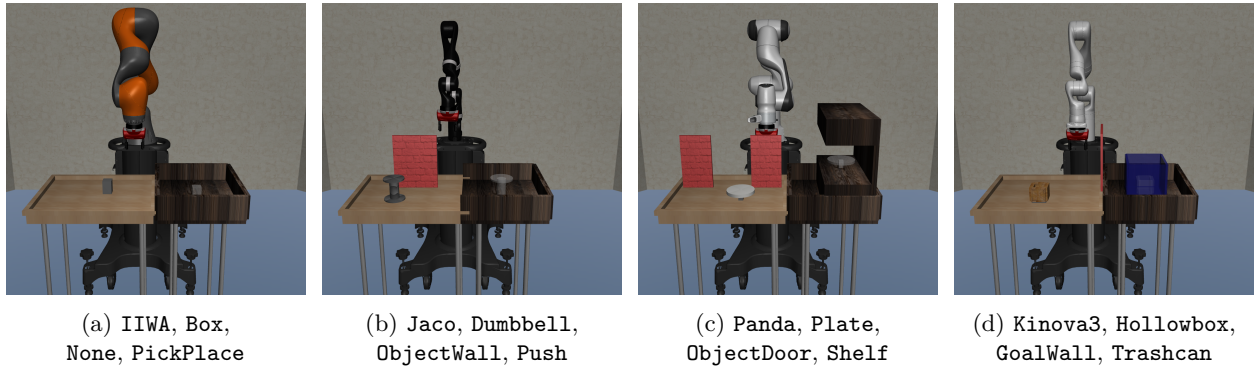


Figure 2: Four example CompoSuite tasks, each defined by selecting one element from each axis.

Robot ID				Object ID				Obstacle ID				Subtask ID			
IIWA	Jaco	Panda	Kinova3	Box	Dumbbell	Plate	Hollow box	None	Object Wall	Object Door	Goal Wall	Pick Place	Push	Shelf	Trash can
Kinova3	Plate	None	Push	→ [0, 0, 0, 1]	[0, 0, 1, 0]	[1, 0, 0, 0]	[0, 1, 0, 0]								

Figure 3: Overview of the 16-dimensional task indicator. For every task in CompoSuite, the model receives a binary vector formed by concatenating four one-hot segments: a 4-dimensional robot ID, 4-dimensional object ID, 4-dimensional obstacle ID, and 4-dimensional subtask ID. Each segment activates exactly one entry corresponding to the chosen element along that axis. The example demonstrates how the task Kinova3, Plate, None, Push is encoded into the final 16-element vector.

## 2.1 CompoSuite Benchmark

CompoSuite (Mendez et al., 2022a) is a simulated robotic manipulation benchmark for evaluating compositional reinforcement learning (RL) agents. CompoSuite provides a family of  $4 \times 4 \times 4 \times 4 = 256$  distinct manipulation tasks by composing exactly one out of four elements from each of the following four axes:

- **Robot arms** KUKA’s IIWA, Kinova’s Jaco, Franka’s Panda, Kinova’s Gen3.
- **Objects** Box, Dumbbell, Plate, Hollow box.
- **Obstacles** No obstacle, Wall blocking object, Doorway near object, Wall blocking goal.
- **Objectives** Pick and place, Push, Place on shelf, Place in trash can.

For each task, states are provided as symbolic representations containing proprioceptive robot features (joint and gripper positions and velocities) together with absolute and relative Cartesian positions of the object, obstacle, and goal in the scene. Each task is defined by selecting exactly one unique element from each of the four axes: Robot, Object, Obstacle, and Objective. To illustrate the compositional structure, Figure 2 shows four example tasks from CompoSuite. The state vector also contains a binary indicator vector of length 16 that identifies a task via four one-hot sub-vectors, one for each axis. Figure 3 illustrates this layout. Rewards are defined with dense, stage-wise rewards to guide the learning.

Hussing et al. (2024) released 1 million transitions for every task in CompoSuite across four dataset variants (approximately 1 billion transitions in total). The four datasets span a range of performance levels, from early training to expert proficiency, and were generated using policies trained with Proximal Policy Optimization (Schulman et al., 2017) and Soft Actor-Critic (Haarnoja et al., 2018). Trajectories are stored as transition tuples  $\langle s, a, r, s', d \rangle$ . For our experiments, we focus exclusively on the expert datasets.

## 2.2 Diffusion Models

A diffusion model is a generative model that learns to reverse a gradual noising process applied to data (Ho et al., 2020). We use diffusion models to generate artificial data for training. More precisely, we use the

Elucidated Diffusion framework (Karras et al., 2022). Given a data vector  $x_0 \in \mathbb{R}^d$ , we consider a collection of noise levels  $\{\sigma_t\}_{t=1}^T$  with  $\sigma_t > 0$ . For each  $t$ , the forward process  $q$  produces a noised sample  $x_t$  by adding Gaussian noise of magnitude  $\sigma_t$ :

$$x_t = x_0 + \sigma_t \varepsilon, \quad \varepsilon \sim \mathcal{N}(0, I), \quad \log \sigma_t \sim \mathcal{N}(P_{\text{mean}}, P_{\text{std}}^2), \quad t = 1, \dots, T,$$

so that, for any fixed noise level  $\sigma_t$ , the conditional distribution of  $x_t$  given  $x_0$  is  $q(x_t | x_0, \sigma_t) = \mathcal{N}(x_0, \sigma_t^2 I)$ . Here,  $P_{\text{mean}} \in \mathbb{R}$  and  $P_{\text{std}} > 0$  are scalar hyperparameters that control the mean and standard deviation of the log-noise distribution  $\log \sigma_t$ . A neural network  $\varepsilon_\theta$  is trained to predict the clean sample  $x_0$  from a noised sample  $x_t$  and its associated noise level  $\sigma_t$ . The training objective is a noise-weighted reconstruction loss:

$$\mathcal{L}_{\text{diff}}(\theta) = \mathbb{E}_{x_0 \sim p_{\text{data}}, \sigma_t, \varepsilon \sim \mathcal{N}(0, I)} \left[ \|\varepsilon_\theta(x_t, \sigma_t) - x_0\|_2^2 w(\sigma_t) \right], \quad w(\sigma) = \frac{\sigma^2 + \sigma_{\text{data}}^2}{(\sigma \sigma_{\text{data}})^2},$$

where  $\sigma_{\text{data}} > 0$  is a hyperparameter representing the typical data scale. At generation time, the model constructs a reverse denoising process over a decreasing sequence of noise levels  $\{\sigma_t\}_{t=1}^T$ . Starting from a high-noise initialization  $x_T \sim \mathcal{N}(0, \sigma_T^2 I)$ , the model iteratively applies the denoiser to define reverse transitions  $p_\theta(x_{t-1} | x_t)$  until it obtains a synthetic sample  $x_0$  that approximately follows the data distribution.

### 3 Task-Graph Compositional Transformer for Iterative Data Generation

We assume a *functionally compositional* task graph. Mendez et al. (2022b) define a hard-coded set of modules, each representing a task element, and define task solutions as fixed paths through that graph. We instead assume that each task consists of basic elements, each of which is a random variable corresponding to one component of the transition, such as a factor of the state or next state, an action, a reward, or a termination indicator. Let  $\mathcal{F}$  denote the set of all such basic elements. Then, each element  $f \in \mathcal{F}$  is associated with an input space  $X^f$  and a representation space  $Y^f$ . An encoder-decoder pair  $(e_f, o_f)$  maps raw variables into the representation space  $e_f : X^f \mapsto Y^f$  and back  $o_f : Y^f \mapsto X^f$ . We define a computation graph  $G = (V, E)$  that captures the shared structure across all tasks, where the vertices  $V = \{Y^f\}_{f \in \mathcal{F}}$  are the representation spaces and the edges  $E$  are transformations that specify how information can flow between representations. A specific MDP  $\mathcal{M}_n$  is characterized by a subset of elements present in that task,  $\mathcal{F}_n \subseteq \mathcal{F}$ , and the induced subgraph of  $G$  on their representation spaces, with a joint distribution over their values. The CompoSuite benchmark fits this view: a task is obtained by selecting one element along the robot, object, obstacle, and objective axes, thereby instantiating a particular set of state-factor vertices and their interactions.

As the graph operates in representation space, it can be used to instantiate a variety of learned functions on an MDP, such as a policy or a conditional generative model. A probabilistic model defined on  $G$  can specify a conditional distribution over the unobserved basic elements given the values of any subset of observed ones.

#### 3.1 Transformers as Graphs

Hard-coding the structure of the computation graph requires extensive domain knowledge and may result in a suboptimal architecture. In consequence, we would like to learn the graph structure directly from data. For this, we rely on the finding that the well-known transformer architecture (Vaswani et al., 2017) can be interpreted as a GNN (Joshi, 2025). In particular, a transformer with  $L$  layers maps a sequence of input tokens  $x_1, \dots, x_K$  to a sequence of output representations  $h_1^L, \dots, h_K^L$  by repeatedly applying self-attention and feed-forward layers. For each token  $i$  and layer  $\ell$ , the model computes queries, keys, and values  $q_i^\ell = W_Q h_i^{\ell-1}$ ,  $k_j^\ell = W_K h_j^{\ell-1}$ ,  $v_j^\ell = W_V h_j^{\ell-1}$  where  $W_Q, W_K, W_V$  are learned weight matrices. The model then assigns the  $i$ -th token's attention weights over each other token  $j$  as  $\alpha_{ij}^\ell = \text{softmax}(q_i^{\ell\top} k_j^\ell / \sqrt{d})$  and aggregates other tokens' values into an updated representation  $h_i^\ell = \text{FF}(\sum_j \alpha_{ij}^\ell v_j^\ell)$ , where  $\text{FF}$  implements a feed-forward layer and  $h_i^0 = x_i$ . In the interpretation of the transformer as a GNN, each token  $i$  corresponds to a node with a feature vector  $h_i^{\ell-1} \in \mathbb{R}_h^d$ , and self-attention implements message passing on a fully connected directed graph over these nodes. By learning the weight matrices  $W_Q, W_K, W_V$ , the transformer learns to assign high attention from token  $i$  to token  $j$  exactly when the graph should contain a strong directed edge from node  $j$  to node  $i$ .

---

Interpreting the transformer as a GNN suggests that a transformer can automatically discover the underlying graph structure of a set of problems that are related compositionally. This reduces the architectural challenge of designing an appropriate graph to designing a tokenization scheme that enables representing such a graph.

### 3.2 Semantic Compositional Diffusion Transformers

Thus, we set out to encode our task graph in a diffusion model by implementing  $\epsilon_\theta$  as a diffusion transformer (DiT; Peebles & Xie, 2023). This model processes noised inputs  $(x_{t,1}, \dots, x_{t,K})$  in the original transition space and outputs denoised predictions  $\epsilon_\theta(x_t, t) \in \mathbb{R}^{K \times d_x}$  at each diffusion step, which is interpreted as a prediction of the added noise for each component. Our diffusion transformer architecture internally uses factor-specific encoders to map inputs to token embeddings, processes these through self-attention, and decodes back to the original space at each step of the reverse diffusion process.

We construct the input sequence for each transition by associating each component of our task graph  $f \in \mathcal{F}$  with the elements of CompoSuite as described in Section 2.1. For both the state and next state, we treat each element per axis as one factor—e.g. each robot arm is one factor. In addition, we add one factor each for the action, reward, and termination signal. This yields a DiT that can learn directly on top of the task graph. For representation learning, we equip each factor with a parametric encoder-decoder pair  $(e_{f,\theta}, o_{f,\psi})$ , both instantiated as neural networks. The encoder maps the inputs into a learned embedding  $y^f = e_{f,\theta}(z^f)$ , which we interpret as living in the representation space  $Y^f$ . The collection  $(y^f)_{f \in \mathcal{F}}$  is treated as the  $K$  tokens processed by the transformer. Self-attention over this factor-specific set of tokens implements graph-compositional inference: at each diffusion step, the representation of every factor  $f$  is updated by attending to all other factors  $f' \in \mathcal{F}$ , so that, for example, the current robot token can condition on the current object, obstacle, and objective tokens in a way that mirrors the edges of  $G = (V, E)$ . At each diffusion step, the transformer outputs denoised token embeddings  $\bar{y}^f$ , which are then mapped back to the original variable domains with the decoders, yielding predictions  $(o_f, \psi(\bar{y}^f))_{f \in \mathcal{F}}$  in the original transition space.

For conditioning, the original DiT injects variables such as the diffusion step  $t$  through adaptive layer normalization. This produces per-block scale and shift parameters that gate the self attention and feed-forward updates. We implement our task conditioning via an additional input embedding that modulates all transformer blocks. For each diffusion step  $t$  and task index  $n$ , we form a context embedding  $u(t, n) = E_t(t) + E_n(n)$  and pass it through a small network that produces adaptive normalization and gating parameters for every block of the DiT. This pathway injects  $(t, n)$  into the model only through these adaptive transforms, and leaves the compositional semantics of the factor-specific tokenization unchanged. The resulting network provides us with a diffusion model that can be trained to generate RL transitions for each task by simply selecting the correct encoders and conditioning. We visualize our proposed architecture in Figure 4.

Using this architecture for diffusion modeling induces a joint representation over factor-specific component embeddings. For each task index  $n$ , the learned diffusion model defines a distribution  $p_\theta(x_0 \mid n)$  over denoised transitions  $x_0$  in the original transition space. Within the denoiser, factor-specific encoders map each component to token embeddings  $(\bar{y}^f)_{f \in \mathcal{F}}$ , the shared diffusion transformer blocks (modulated by task conditioning through adaptive layer normalization) process these through self-attention to learn relationships between factors, and decoders map the embeddings back to the original space. As this joint representation over component embeddings is shared across tasks, we can use structure learned from one task to improve the marginals for others and incrementally refine each factor’s predictive distribution as new tasks are added.

### 3.3 Self-Refining Compositional Distributions

We use our trained DiT to produce training data for two purposes: training behavior policies for unseen tasks (for which we do not have real training data), and updating the DiT itself. By virtue of the compositional graph structure, our model can train on a set of compositional tasks, generate data for new task combinations zero-shot, and use the generated data to improve the DiT. Notably, because we learn factorized pieces of a distribution to improve their marginals, the generator improves not only on the tasks for which we generate data, but also on tasks that share some of these factors. As an illustrative example, consider tasks that vary on the robot and object (e.g., a subset of CompoSuite). Suppose the dataset contains transitions for three tasks: **(Panda, Box)**, **(Jaco, Box)**, and **(Panda, Plate)**, but no real data for **(Jaco, Plate)**. Our compositional

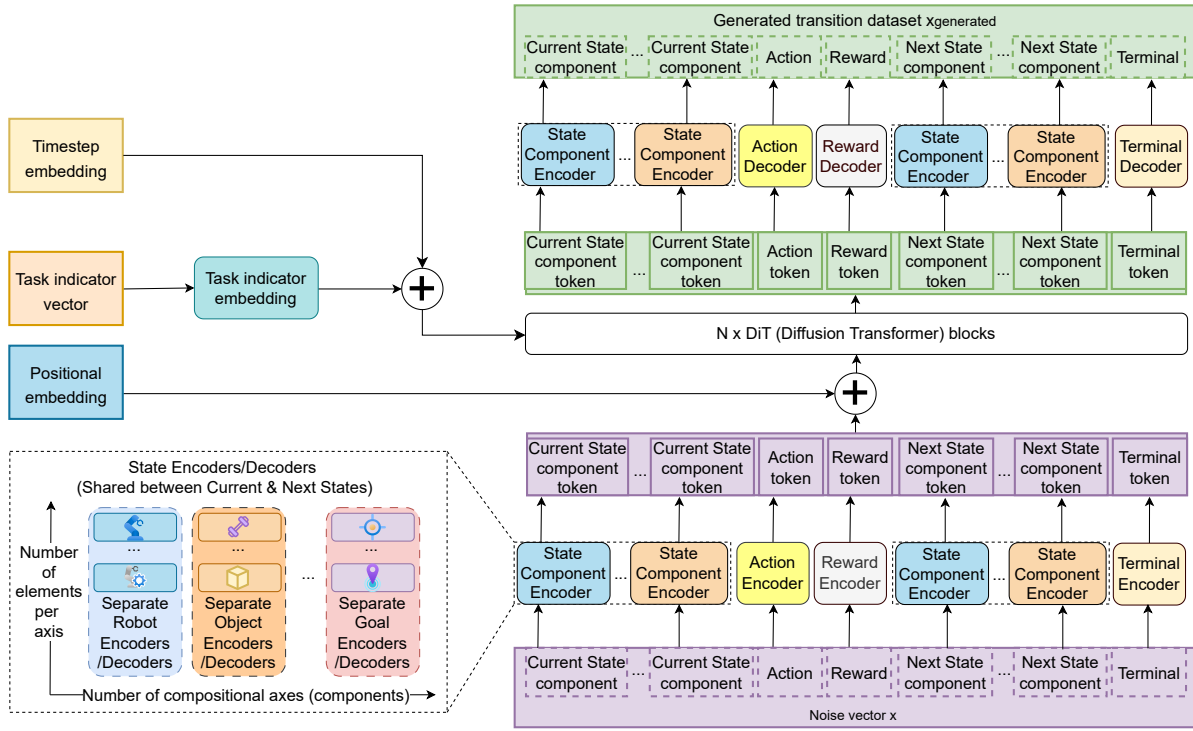


Figure 4: Visualization of our semantic compositional transformer architecture. We factorize each transition into state factors, actions, reward, and terminal indicators. State factors represent the compositional dimensions along which tasks can vary (for example, different robots). Each state factor has its own encoder-decoder pair, providing partial parameter separation. The encoded tokens, augmented with positional embeddings, are processed by several diffusion transformer layers. The diffusion transformer uses adaptive statistics conditioned on timestep and task indicator embeddings. Its output tokens are then decoded by the factor-specific decoders, with state encoder-decoder pairs shared between current and next state.

DiT can generate plausible transitions for **(Jaco, Plate)** by combining the learned **Jaco** and **Plate** factors. Retraining on these additional samples increases the effective data available for the shared **Plate** factor and constrains it across multiple robotic contexts, so that any downstream task involving **Plate** —e.g., **(IIWA, Plate)**—benefits from a sharper object marginal than would be possible from the original tasks alone.

We summarize our procedure in Algorithm 1. The algorithm starts with a set of (real) data from a sub-set of training tasks and proceeds in rounds. In every round, we fit our DiT to all training data. We then generate data for all existing validation and test tasks, train a policy using TD3-BC (Fujimoto & Gu, 2021) on the generated data, and evaluate the policy online in the environment. If the success rate (sr) for any task is larger than some threshold  $\tau$ , we add the data generated for this task to the training set. This performance-based filter only admits synthetic data that is useful for training high-quality policies. If no tasks surpass the quality threshold, we increase a patience parameter  $c$ . When the patience exceeds a predefined threshold  $C$ , we decrease the quality threshold  $\tau$ .

The approach in Algorithm 1 uses self-generated data to train a data generator. One question is whether adding sub-optimal data for a single task might lead to degraded performance across all tasks. Training on iteratively generated data of prior versions of a generative model often results in the performance of the model decreasing over time, a phenomenon known as model collapse (Shumailov et al., 2024). Our compositional transformer architecture from Section 3.2 uses the data generated for a particular task exclusively to train the encoder-decoder pairs specific to that task’s elements. In consequence, each generated dataset contributes only to a subset of all transformer weights (e.g., data generated for the **Panda** encoder-decoder is not used

---

**Algorithm 1** Compositional Iterative Bootstrapping with Synthetic Data

---

**Require:** Initial dataset  $\mathcal{D}$ ; target task set  $\mathcal{T}_{\text{target}}$ ; initial threshold  $\tau_0$  with lower bound  $\tau_{\min}$ ; threshold step size  $\Delta_\tau$ ; patience  $C$ ; maximum iterations  $K$

1:  $\mathcal{D}_{\text{train}}^{(0)} \leftarrow \mathcal{D}$ ,  $\mathcal{T}_{\text{solved}}^{(0)} \leftarrow \emptyset$ ,  $\tau \leftarrow \tau_0$ ,  $c \leftarrow 0$

2: **for**  $k = 0, 1, \dots, K$  **do**

3:   Train diffusion model  $\varepsilon_\theta^{(k)}$  on  $\mathcal{D}_{\text{train}}^{(k)}$

4:   **for all**  $t \in \mathcal{T}_{\text{target}} \setminus \mathcal{T}_{\text{solved}}^{(k)}$  **do**

5:     Generate synthetic data  $\mathcal{D}_{\text{syn}}^{(k)}(t)$  using  $\varepsilon_\theta^{(k)}$

6:     Train and evaluate TD3-BC policy  $\pi_\phi^{(k)}(t)$  on  $\mathcal{D}_{\text{syn}}^{(k)}(t)$  to obtain success rate  $\text{sr}^{(k)}(t)$

7:   **end for**

8:    $\mathcal{T}_{\text{solved}}^{(k+1)} \leftarrow \mathcal{T}_{\text{solved}}^{(k)} \cup \{t : \text{sr}^{(k)}(t) > \tau\}$

9:   **if**  $\mathcal{T}_{\text{solved}}^{(k+1)} = \mathcal{T}_{\text{solved}}^{(k)}$  **then**  $c \leftarrow c + 1$  **else**  $c \leftarrow 0$  **end if**

10:   **if**  $c \geq C$  **then**  $\tau \leftarrow \max(\tau - \Delta_\tau, \tau_{\min})$ ,  $c \leftarrow 0$  **end if**

11:    $\mathcal{D}_{\text{train}}^{(k+1)} \leftarrow \mathcal{D} \cup \bigcup_{t \in \mathcal{T}_{\text{solved}}^{(k+1)}} \mathcal{D}_{\text{syn}}^{(k)}(t)$

12:   **if**  $\mathcal{T}_{\text{target}} \subseteq \mathcal{T}_{\text{solved}}^{(k+1)}$  **then break** **end if**

13: **end for**

14: **return**  $\varepsilon_\theta^{(k)}, \{\pi_\phi^{(k)}(t)\}_{t \in \mathcal{T}_{\text{target}}}, \mathcal{T}_{\text{solved}}^{(k)}, \mathcal{D}_{\text{train}}^{(k)}$

---

to update the parameters of the Jaco encoder-decoder). This mechanism inherent to our compositional architecture partially guards our DiT against model collapse.

## 4 Experimental Evaluation of the Semantic Compositional Transformer

This section empirically evaluates our compositional transformer for generating robotic data of unseen tasks. Because our algorithm generates millions of synthetic transition tuples for each task, we restrict our experiments to a subset of 64 tasks of the CompoSuite benchmark, chosen by using one fixed robot arm: IIWA. We consider a setting where we only have training data for 14 of the 64 tasks, which we show empirically to be insufficient for zero-shot generalization of a non-compositional data-generating baseline (Appendix A). We use our method to iteratively generate data for the remaining 50 tasks, and report performance on a test set consisting of 32 of the 50 held-out tasks. Note that Algorithm 1 requires online evaluation on the zero-shot tasks, for which we perform 10 trajectory rollouts per task (500 transitions per rollout) every round.

### 4.1 Baselines

We first compare against two static offline RL approaches, which cannot generate data for new tasks, to demonstrate the value of iterative data generation.

- **Hardcoded Compositional RL** We train the multi-task compositional architecture of Mendez et al. (2022a) via offline RL using TD3-BC. This architecture was designed specifically to solve CompoSuite tasks, but it employs a hard-coded compositional structure.
- **Semantic Compositional RL** To test the benefits of learned connections in compositional representations, we also implement a semantic compositional RL approach based on our architecture. We use TD3-BC to train a multi-task model which uses our semantic compositional transformer for the encoder. However, rather than decoding each element with its own decoder, we use mean pooling over all output tokens and process the concatenated vector with an additional feed-forward layer to obtain an action.

We then consider three baseline architectures that iteratively generate data per Algorithm 1.

- **Monolithic** To highlight the difficulty of compositional generalization for monolithic architectures, we consider a variant of Synthetic Experience Replay (SynthER; Lu et al., 2023). SynthER trains a diffusion model on the data collected by an off-policy RL algorithm (e.g., TD3) to augment the RL batch with artificial transitions. We are specifically interested in the neural network architecture for diffusion, as it

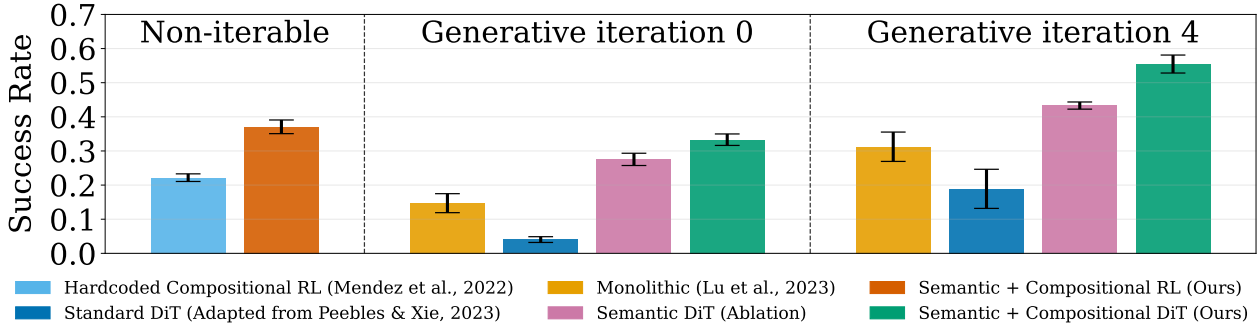


Figure 5: Zero-shot success rate for non-iterable RL models and RL models trained on synthetic data of a generative model at iteration iteration 0, and best zero-shot success rate for RL models trained on synthetic of a generative model after 4 iterations of self-improvement. Overall, the semantic compositional architecture leads to large improvements in the RL as well as generative model setting. (Left) The semantic compositional architecture improves over the hard-coded compositional RL architecture by almost doubling the success rate. (Middle) In the generative model setting, the semantic tokenization approaches beat the architectures that are not adapted to the task. (Right) After 4 rounds of self-improvement, the semantic compositional DiT method achieves highest performance across all other approaches.

has shown promise for generating useful transitions for RL training. In particular, SynthER employs a monolithic architecture that parametrizes the diffusion denoiser  $\epsilon_\theta$  via several residual feed-forward layers. We adapt this architecture to the multi-task setting by conditioning the denoiser  $\epsilon_\theta$  on the task indicator. At each layer, the noisy transition is augmented by additive embeddings encoding both timestep and task information  $\tilde{x}_t = x_t + E_t(t) + E_c(c)$ , where  $E_t(t)$  encodes the diffusion timestep through sinusoidal features and  $E_c(c)$  linearly projects the multi-hot task indicator into the same latent space. This conditioning strategy injects task information into the residual computation without modifying the architecture.

- **Standard DiT** We then compare against a standard DiT without semantic or compositional tokenization (Peebles & Xie, 2023). This DiT simply chops the input into patches of roughly size 15 and computes the tokens using a shared encoder. This yields a transformer with the same amount of tokens as our compositional semantic encoder but without compositional structure.
- **Semantic DiT** Our tokenization scheme splits the input into semantic patches (e.g., robot state, object state, action) and uses a separate encoder-decoder pair for each element (e.g., one for the IIWA and one for the Jaco). To verify the need to train separate encoder-decoders to learn the different representation spaces for each element, we compare against a DiT that splits the input into semantic patches but trains one shared encoder-decoder across elements of an axis (e.g., one for all robots). While this carries the semantic meaning of the input, it does not model the nodes that constitute the CompoSuite task graph.

In each round of data generation, the diffusion model generates data for the held-out tasks that have not surpassed the threshold  $\tau$  (i.e., unseen tasks for the diffusion model). We use the generated data to train task-specific RL policies using TD3-BC for 50,000 steps, rolling out 10 evaluation trajectories every 5,000 steps. We keep the best-performing policy for a task across evaluation steps and data generation iterations.

## 4.2 Zero-shot Generalization

To verify the zero-shot abilities of our approach, we pre-train all models on the training tasks and report success on the held-out test tasks. RL baselines directly use a zero-shot policy, while diffusion approaches generate synthetic data and train policies on the generated data. We also run four iterations of iterative self-improvement (Algorithm 1) on diffusion approaches. Performance of RL algorithms is averaged across tasks over 15 seeds. For generative models, we keep the best-performing policy across the four iterations. We train the diffusion model over three independent seeds, and for each seed we train the policies over five RL training seeds; we report the average across tasks, diffusion seeds, and RL seeds. Error bars indicate standard error across 15 RL seeds and three diffusion seeds. We report the results in Figure 5.

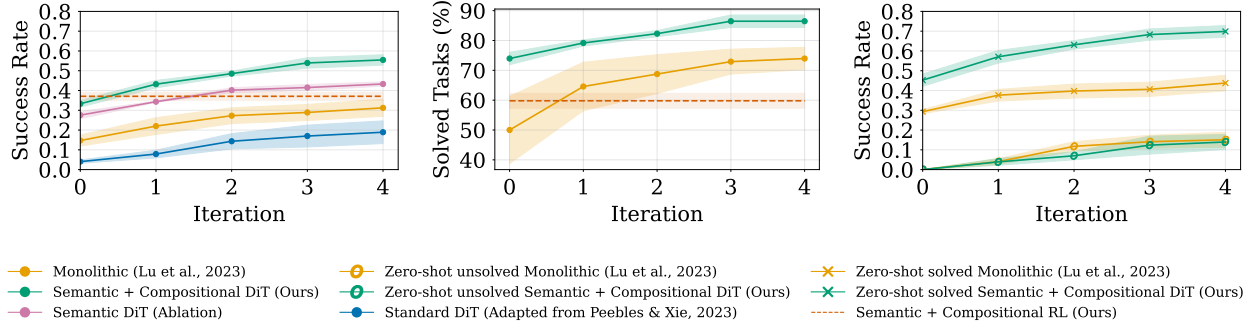


Figure 6: Performance of different diffusion architectures over iterations of our self-improvement procedure. (Left) Zero-shot best success rate achieved so far. RL agents trained on synthetic data from the semantic compositional diffusion architecture consistently achieve higher success rates than agents trained on data from all other diffusion architectures and quickly surpass the semantic compositional RL baseline. (Middle) Number of tasks solved at least once across iterations: RL trained on synthetic data from the semantic compositional diffusion transformer outperforms both baselines and solves nearly all tasks at least once. (Right) Zero-shot best success rate achieved so far, separated by initial task difficulty. Tasks are partitioned into those that exhibit non-zero success at iteration 0 and those that were entirely unsolved. The semantic compositional architecture particularly improves performance on tasks on which it already obtains initial success in iteration 0. Shaded regions indicate standard error over 3 diffusion seeds.

**Reinforcement learning performance** The compositional RL baseline of Mendez et al. (2022a), which was specifically designed for these tasks, achieves some zero-shot generalization. However, the composition learned by our compositional transformer succeeds twice as often. This provides evidence that our architecture can extract meaningful compositional structure from data. The improved performance suggests that the graph structure learned by our architecture more effectively connects relevant vertices than the hard-coded architecture of Mendez et al. (2022a).

**Initial generative performance** After the first round of training the first diffusion models, RL based on the data generated by the monolithic architecture performs worse than all compositional variants (RL or diffusion), demonstrating the usefulness of composition for efficient zero-shot data generation. The standard DiT model performs worst across all models, indicating that a proper tokenization of the input space is needed. In consequence, any improvement from our method is not a direct result of the transformer being a stronger representation learning architecture. Our semantic compositional data generation process performs nearly on par with the semantic compositional RL baseline. Critically, as we discuss next, the DiT can then generate data for new tasks and iteratively improve its own performance.

**Iterated generative performance** Our iterative self-improvement algorithm increases all architectures’ success rates. The monolithic architecture improves by 17%, standard DiT by 15%, semantic DiT by 16%, and semantic compositional DiT by 22%—the semantic compositional architecture achieves the largest absolute improvement. These marked improvements indicate that the nature of compositional data is useful for out-of-distribution generation. As our approach can self-improve, it quickly outperforms the static RL baseline without any additional real training data. Note that we can view the threshold  $\tau$  as a soft upper bound on success rate, since we generate data that enables as little as  $\tau$  success rate per task, and it is challenging to train policies that outperform this level of data quality. With  $\tau$  reaching 0.7 at iteration four and our semantic compositional DiT achieving a success rate of 55%, the gap to this soft upper bound closes.

### 4.3 Iterative Compositional Data Generation

Next, we investigate each round of the iterative procedure for data generation. In every round of Algorithm 1, we evaluate five runs of TD3-BC for each unsolved task ( $sr < \tau$ ) to average out the randomness from RL training and track the best success rate so far for each task. Figure 6 reports the average success rate in every iteration and the number of tasks that achieve success at least once (i.e.  $sr > 0$ ).

---

**Success rate over time** Figure 6 (left) reiterates the finding that all architectures consistently improve when artificial data is added. All architectures improve at a similar rate, and so the fact that only semantic architectures eventually outperform the RL version of our architecture is largely due to their significantly higher initial success rate. Our compositional semantic architecture only requires one round of self-improvement to exceed the performance of its RL counterpart. This interplay between initial generative performance and downstream RL performance highlights the importance of studying the two in tandem.

**Solved tasks over time** Figure 6 (middle) shows that the semantic compositional approach generates data that yields at least one successful trajectory more consistently than the monolithic approach. In addition, after four iterations of refinement, we solve almost every task at least once. This suggests that our approach could serve as a powerful starting point for fine-tuning new policies, since it can drastically reduce the exploration challenge of online RL. Interestingly, while RL using our architecture achieves a higher zero-shot success rate than our generative approach at iteration 0, this success rate is concentrated on a smaller fraction of tasks. This suggests that the diffusion model generalizes more broadly across tasks, but the initial data quality is insufficient to extract good policies in all parts of the state space.

Given that the semantic compositional model yields the most significant improvement in total success but also has a smaller improvement on tasks solved, one might conclude that our architecture is better at iteratively deriving information from successful tasks by refining marginals. To verify this, we analyze whether iterative improvements appear on tasks that see some success or tasks that are not yet solved. In Figure 6 (right), we show that the monolithic architecture improves roughly at the same rate on both the already successful and unsuccessful tasks. While our semantic compositional model also improves in both regimes, it obtains a much larger jump in performance on tasks that see some initial success at iteration 0. In part, this stems from the fact that there are few tasks left on which no success is achieved initially. Yet, it also provides evidence that our semantic compositional model improves encoder-decoder pairs point-wise using self-generated data.

#### 4.4 Analyzing Compositional Structure

This section studies the compositional structure learned by our architecture. As discussed in Section 2.2, we use the Elucidated Diffusion approach (Karras et al., 2022), which parameterizes the diffusion process using continuous noise levels  $\sigma$  rather than discrete timesteps, with default noise range  $\sigma \in [\sigma_{\min}, \sigma_{\max}]$ . For our analysis, we evaluate the model’s behavior at a noise level  $\sigma_{\text{midpoint}}$  corresponding to the midpoint of the generation schedule, computed per the sampling schedule formula (Karras et al., 2022):

$$\sigma_{i < N} = \left( \sigma_{\max}^{1/\rho} + \frac{i}{N-1} \left( \sigma_{\min}^{1/\rho} - \sigma_{\max}^{1/\rho} \right) \right)^{\rho}, \quad \sigma_N = 0,$$

where  $i$  denotes the step.  $\sigma_{\text{midpoint}}$  represents a moderate noise level the model encounters during generation. Throughout this section, we use the DiT trained at iteration 0, using only real data.

**Intervention influence** To analyze the compositional dependencies that our model learns, we compute an influence matrix that measures how inputs to each encoder module affect the outputs of each decoder module. For a given task, we generate random Gaussian noise inputs and compute the outputs at  $\sigma_{\text{midpoint}}$ . We then systematically intervene on each encoder module by zeroing out its output patches and measure the resulting change in each decoder module’s output. The influence of encoder module  $i$  on decoder module  $j$  is quantified as the  $L_2$  norm of the normalized difference between the intervened and nominal decoder outputs. Averaging these normalized differences across many noise samples yields an influence matrix whose entries quantify the causal effect of one module on another while remaining comparable across decoders of different dimensionality. This allows us to measure, for example, which predictions are most affected if the object information is missing. Figure 7 presents the average intervention influence matrix over all training tasks.

As expected, the largest deviations happen on the diagonal, as masking a certain element at the encoder makes it difficult to accurately generate that element itself. For example, if the object embedding is masked, the transformer relies exclusively on task conditioning to generate object information. Variations across state components further expose a particular dependency structure among elements. For instance, task

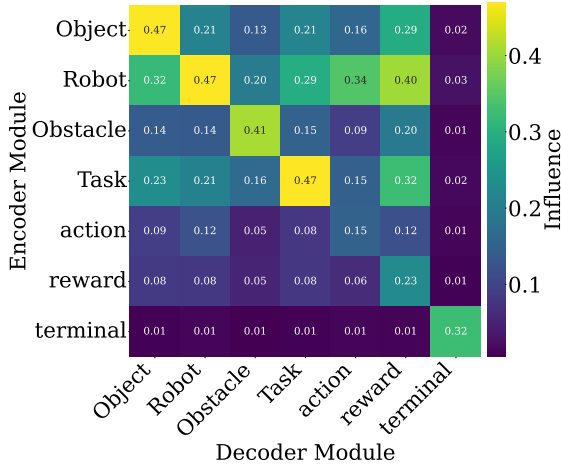


Figure 7: Average intervention influence over all training tasks. The heatmap shows how masking each encoder module (rows) changes the predictions produced by each decoder module (columns). Brighter values indicate a larger influence. The plot shows strong diagonal effects, meaning each factor depends most on its own encoder, but it also reveals notable cross-factor interactions. In particular, the robot encoder has a strong effect on several other decoders, especially the reward decoder.

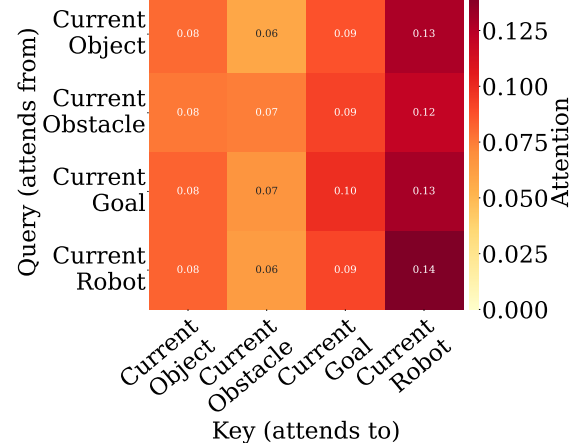


Figure 8: Average attention weights over all training tasks for a single block diffusion transformer. The heatmap shows how much each state component encoder (rows) attends to every other component (columns) when generating denoised representations. Darker colors indicate stronger attention. The plot shows a clear ordering in which the robot component receives the strongest attention from all queries, followed by the goal, the object, and finally the obstacle.

input influences object prediction more than it does obstacle prediction. Yet all components depend on each other to some degree. This is not particularly surprising, since the state representation contains relative information (e.g., relative poses). More interestingly, many decoder outputs rely heavily on the robot arm encoding. This highlights the crucial importance of the robot arm in our model for generating data. The largest influence outside the diagonal is for the robot arm input and reward prediction. In general, the reward predictions greatly depend on the state components but not so much on the action, which is correctly inferred by the model since the reward in CompoSuite is only a function of the state. The terminal signal depends exclusively on its own input, since the dataset released by Hussing et al. (2024) contains expert trajectories for almost all tasks, making failure terminations rare in the training data.

**Attention masks** Now, we shift our focus to the state encoder structure, the central piece of our architecture design. We study the DiT attention structure by capturing the full  $11 \times 11$  self-attention matrices. To inspect which encoder outputs map to which decoders, we trained a single-layer transformer. We draw 100 Gaussian inputs, run the model at  $\sigma_{\text{midpoint}}$ , and compute per-head attention weights from every Multi-Head Self-Attention block. We do this for the 14 training tasks and average across samples and attention heads. We are mostly interested in the state decomposition, which is the main distinguishing feature of our architecture. Figure 8 shows the entries of the attention matrix corresponding to state elements.

The state attention mask reveals that there exists a non-trivial mapping between the state encoder and decoder pairs. First, every decoder pays some attention to its corresponding encoder (the diagonal). Then, we observe an ordering of importance across state elements. Every encoder pays greatest attention to the robot, then the objective, then the object, then the obstacle. The ordering we find is contrary to the hard-coded architecture of Mendez et al. (2022a), where the robot modules are stacked onto the remaining modules last, implying that other encoders cannot access robot information. This difference may be stem from fundamentally different computations required to learn an RL policy compared to generating RL data.

---

## 5 Related Work

**Compositional Generalization in Robotics and RL** In robotics, compositional generalization has been pursued through a variety of mechanisms. Some approaches introduce modularity or architectural biases aimed at composing semantic units such as instructions or high-level skills (Xu et al., 2018; Devin et al., 2019; Kuo et al., 2020; Wang et al., 2023). Other work targets the control layer directly, designing modular, factorized, or entity-centric policy architectures that encourage reuse of behavioral components across tasks (Devin et al., 2017; Mendez et al., 2022b; Zhou et al., 2025). Some approaches seek to automatically identify and decompose policies into functional modules (Yang et al., 2020; Mittal et al., 2020; Goyal et al., 2021). A complementary direction exploits scene-centric formulations that use structured object-relational representations to compose low-level visuomotor skills in novel physical configurations (Qi et al., 2025).

These approaches demonstrate the importance of leveraging task structure, but they typically assume a *hand-designed* decomposition of robots, objects, and goals. In contrast, our method learns this structure *directly from data* by interpreting a diffusion transformer as a GNN and equipping it with factor-specific tokenizers. Whereas prior work uses compositionality to structure *policies*, we instead use it to structure a *generative model of transitions*, enabling zero-shot synthesis of data for unseen task compositions.

**Generated Data in Robotics and RL** Synthetic data has become a key idea for scaling robotic learning. One line of work expands imitation datasets through trajectory-level augmentations, where expert demonstrations are perturbed, resampled, or regenerated to increase coverage (Mandlekar et al., 2023; Wang et al., 2024; Ameperosa et al., 2025; Jiang et al., 2025). Although these methods enrich demonstration sets, they remain constrained to variations of the same underlying tasks without expanding into *new compositions*.

Complementary efforts in reinforcement learning explore *generative replay*, where learned generative models synthesize transitions to supplement or replace entries in an agent’s replay buffer (Huang et al., 2017; Ludjen, 2021; Imre, 2021; Lu et al., 2023; Voelcker et al., 2025). As generative modeling techniques have advanced—from variational autoencoders (Kingma & Welling, 2014) and generative adversarial networks (Goodfellow et al., 2014) to, more recently, diffusion models (Karras et al., 2022)—the fidelity of replayed experience and the sample efficiency of these approaches have improved accordingly. However, these methods still generate data only for the *same tasks* observed during training. They do not attempt to produce transitions for *unseen combinations of factors* that fall outside the original task distribution.

Another orthogonal direction emphasizes visual augmentation, including render-driven and vision-only pipelines that procedurally generate synthetic video datasets (Bonetto et al., 2023; Singh et al., 2024; Yu et al., 2024; Han et al., 2025; Yu et al., 2025), as well as generative and diffusion-based methods that augment images while holding actions constant (Chen et al., 2023; Yu et al., 2023). While effective for increasing visual diversity, these approaches do not provide transition-level data reflecting novel task semantics.

Our work is complementary to all of these efforts but differs fundamentally: we generate full state-action-next-state transitions for *unseen* tasks. Moreover, our iterative procedure evaluates the usefulness of generated data via offline RL, creating a closed-loop mechanism for self-improving compositional data generation.

**Compositional Data Generation in Robotics** Recent work has shown that exposing robots to compositional factors of variation can significantly improve generalization and reduce data requirements in manually collected datasets (Gao et al., 2024). In parallel, compositional generative models have emerged that synthesize novel object and task combinations to expand the space of training experience (Zhou et al., 2024; Barcellona et al., 2025). These approaches demonstrate the utility of factoring environments into reusable components, but they operate on image representations and often rely on predefined decompositions. More importantly, prior compositional generative approaches do not address the challenge of improving a generative model using its own compositional synthesized data. In contrast, our approach introduces an *iterative self-refinement procedure* in which the generative model synthesizes transitions for unseen task compositions.

## 6 Conclusion

In this work, we introduce an iterative compositional data generation framework that uses a semantic compositional diffusion transformer and a self-improvement loop to synthesize and curate manipulation data.

---

This data is of sufficient quality to train policies that solve novel combinations of compositional tasks. Our work shows that compositional data generation can turn limited real interaction into policies that generalize across many tasks. This has the potential to reduce data collection and engineering costs for real-world robotic systems, making it easier to deploy flexible manipulation skills in diverse environments.

At present, our method decides whether a generated task dataset is added to the training pool by running an online evaluation loop. We deploy an RL agent on the newly generated task and include the corresponding data only if its success rate exceeds a fixed threshold. This makes our procedure dependent on online interaction with the environment, which can be costly in many real-world settings. Note that our approach is not tied to this particular choice and any suitable scoring function that assesses the utility of generated data could be used instead. An important direction for future work is to replace this online evaluation with interaction-free or partially offline proxies that can reliably predict the utility of newly generated data.

---

## Acknowledgments

DSB acknowledges support from the Center for Curiosity. MH and EE were partially supported by the Army Research Office under MURI award W911NF201- 0080 and DARPA award HR00112420305. Any opinions, findings, conclusions, or recommendations expressed in this material are those of the authors and do not necessarily reflect the view of DARPA, the US Army, or the US government.

## References

Ezra Ameperosa, Jeremy A. Collins, Mrinal Jain, and Animesh Garg. Rocoda: Counterfactual data augmentation for data-efficient robot learning from demonstrations. In *IEEE International Conference on Robotics and Automation*, 2025.

Jacob Andreas, Dan Klein, and Sergey Levine. Modular multitask reinforcement learning with policy sketches. In *Proceedings of the 34th International Conference on Machine Learning*, 2017.

Leonardo Barcellona, Andrii Zadaianchuk, Davide Allegro, Samuele Papa, Stefano Ghidoni, and Efstratios Gavves. Dream to manipulate: Compositional world models empowering robot imitation learning with imagination. In *The Thirteenth International Conference on Learning Representations*, 2025.

Elia Bonetto, Chenghao Xu, and Aamir Ahmad. Learning from synthetic data generated with grade. In *Pretraining for Robotics Workshop, IEEE International Conference on Robotics and Automation*, 2023.

Zoey Chen, Sho Kiami, Abhishek Gupta, and Vikash Kumar. Genaug: Retargeting behaviors to unseen situations via generative augmentation. *arXiv preprint arXiv:2302.06671*, 2023.

Coline Devin, Abhishek Gupta, Trevor Darrell, Pieter Abbeel, and Sergey Levine. Learning modular neural network policies for multi-task and multi-robot transfer. In *Proceedings of the 2017 IEEE International Conference on Robotics and Automation (ICRA-17)*, pp. 2169–2176, 2017.

Coline Devin, Daniel Geng, Pieter Abbeel, Trevor Darrell, and Sergey Levine. Plan arithmetic: Compositional plan vectors for multi-task control. In *Advances in Neural Information Processing Systems (NeurIPS)*, 2019.

Scott Fujimoto and Shixiang Shane Gu. A minimalist approach to offline reinforcement learning. In *Advances in Neural Information Processing Systems (NeurIPS)*, 2021.

Jensen Gao, Annie Xie, Ted Xiao, Chelsea Finn, and Dorsa Sadigh. Efficient data collection for robotic manipulation via compositional generalization. In *Proceedings of Robotics: Science and Systems (RSS)*, 2024.

Ian Goodfellow, Jean Pouget-Abadie, Mehdi Mirza, Bing Xu, David Warde-Farley, Sherjil Ozair, Aaron Courville, and Yoshua Bengio. Generative adversarial nets. In *Advances in Neural Information Processing Systems (NeurIPS)*, 2014.

Anirudh Goyal, Alex Lamb, Jordan Hoffmann, Shagun Sodhani, Sergey Levine, Yoshua Bengio, and Bernhard Schölkopf. Recurrent independent mechanisms. In *Proceedings of the International Conference on Learning Representations (ICLR)*, 2021.

Tuomas Haarnoja, Aurick Zhou, Pieter Abbeel, and Sergey Levine. Soft actor-critic: Off-policy maximum entropy deep reinforcement learning with a stochastic actor. In *Proceedings of the 35th International Conference on Machine Learning (ICML)*, 2018.

Xiaoshen Han, Minghuan Liu, Yilun Chen, Junqiu Yu, Xiaoyang Lyu, Yang Tian, Bolun Wang, Weinan Zhang, and Jiangmiao Pang. Re3sim: Generating high-fidelity simulation data via 3d-photorealistic real-to-sim for robotic manipulation. *arXiv preprint arXiv:2502.08645v3*, 2025.

Jonathan Ho, Ajay Jain, and Pieter Abbeel. Denoising diffusion probabilistic models. In *Advances in Neural Information Processing Systems*, 2020.

---

Vincent Huang, Tobias Ley, Martha Vlachou-Konchylaki, and Wenfeng Hu. Enhanced experience replay generation for efficient reinforcement learning. *arXiv preprint arXiv:1705.08245*, 2017.

Marcel Hussing, Jorge A. Mendez, Anisha Singrodia, Cassandra Kent, and Eric Eaton. Robotic manipulation datasets for offline compositional reinforcement learning. In *Reinforcement Learning Conference*, 2024.

Baris Imre. An investigation of generative replay in deep reinforcement learning. Thesis, University of Twente, Enschede, January 2021.

Michael Janner, Yilun Du, Joshua Tenenbaum, and Sergey Levine. Planning with diffusion for flexible behavior synthesis. In *Proceedings of the 39th International Conference on Machine Learning*, 2022.

Zhenyu Jiang, Yuqi Xie, Kevin Lin, Zhenjia Xu, Weikang Wan, Ajay Mandlekar, Linxi “Jim” Fan, and Yuke Zhu. Dexmimicgen: Automated data generation for bimanual dexterous manipulation via imitation learning. In *IEEE International Conference on Robotics and Automation*, 2025.

Chaitanya K. Joshi. Transformers are graph neural networks. *arXiv preprint arXiv:2506.22084*, 2025.

Tero Karras, Miika Aittala, Timo Aila, and Samuli Laine. Elucidating the design space of diffusion-based generative models. In *Advances in Neural Information Processing Systems (NeurIPS)*, 2022.

Alexander Khazatsky, Karl Pertsch, Suraj Nair, Ashwin Balakrishna, Sudeep Dasari, Siddharth Karamcheti, Soroush Nasiriany, Mohan Kumar Srirama, Lawrence Yunliang Chen, Kirsty Ellis, Peter David Fagan, Joey Hejna, Masha Itkina, Marion Lepert, Yecheng Jason Ma, Patrick Tree Miller, Jimmy Wu, Suneel Belkhale, Shivin Dass, Huy Ha, Arhan Jain, Abraham Lee, Youngwoon Lee, Marius Memmel, Sungjae Park, Ilija Radosavovic, Kaiyuan Wang, Albert Zhan, Kevin Black, Cheng Chi, Kyle Beltran Hatch, Shan Lin, Jingpei Lu, Jean Mercat, Abdul Rehman, Pannag R Sanketi, Archit Sharma, Cody Simpson, Quan Vuong, Homer Rich Walke, Blake Wulfe, Ted Xiao, Jonathan Heewon Yang, Arefeh Yavary, Tony Z. Zhao, Christopher Agia, Rohan Baijal, Mateo Guaman Castro, Daphne Chen, Qiyu Chen, Trinity Chung, Jaimyn Drake, Ethan Paul Foster, Jensen Gao, David Antonio Herrera, Minho Heo, Kyle Hsu, Jiaheng Hu, Donovon Jackson, Charlotte Le, Yunshuang Li, Roy Lin, Zehan Ma, Abhiram Maddukuri, Suvir Mirchandani, Daniel Morton, Tony Nguyen, Abigail O’Neill, Rosario Scalise, Derick Seale, Victor Son, Stephen Tian, Emi Tran, Andrew E. Wang, Yilin Wu, Annie Xie, Jingyun Yang, Patrick Yin, Yunchu Zhang, Osbert Bastani, Glen Berseth, Jeannette Bohg, Ken Goldberg, Abhinav Gupta, Abhishek Gupta, Dinesh Jayaraman, Joseph J Lim, Jitendra Malik, Roberto Martín-Martín, Subramanian Ramamoorthy, Dorsa Sadigh, Shuran Song, Jiajun Wu, Michael C. Yip, Yuke Zhu, Thomas Kollar, Sergey Levine, and Chelsea Finn. DROID: A Large-Scale In-The-Wild Robot Manipulation Dataset. In *Proceedings of Robotics: Science and Systems*, Delft, Netherlands, July 2024. doi: 10.15607/RSS.2024.XX.120.

Diederik P Kingma and Max Welling. Auto-encoding variational bayes. In *International Conference on Learning Representations (ICLR)*, 2014.

Yen-Ling Kuo, Boris Katz, and Andrei Barbu. Deep compositional robotic planners that follow natural language commands. In *Proceedings of the IEEE International Conference on Robotics and Automation (ICRA)*, 2020.

Zhixuan Liang, Yao Mu, Mingyu Ding, Fei Ni, Masayoshi Tomizuka, and Ping Luo. Adaptdiffuser: Diffusion models as adaptive self-evolving planners. In *International Conference on Machine Learning*, pp. 20725–20745. PMLR, 2023.

Cong Lu, Philip J. Ball, Yee Whye Teh, and Jack Parker-Holder. Synthetic experience replay. In *Thirty-seventh Conference on Neural Information Processing Systems*, 2023.

Arflyno Chrisdion Pahombar Ludjen. Generative replay in deep reinforcement learning. Thesis, University of Twente, Enschede, June 2021.

Ajay Mandlekar, Soroush Nasiriany, Bowen Wen, Iretiayo Akinola, Yashraj Narang, Linxi Fan, Yuke Zhu, and Dieter Fox. Mimicgen: A data generation system for scalable robot learning using human demonstrations. In *Conference on Robot Learning*, 2023.

---

Jorge A. Mendez, Marcel Hussing, Meghna Gummadi, and Eric Eaton. Composuite: A compositional reinforcement learning benchmark. In *Proceedings of The 1st Conference on Lifelong Learning Agents*, volume 199 of *Proceedings of Machine Learning Research*, pp. 982–1003. PMLR, 22–24 Aug 2022a.

Jorge A Mendez, Harm van Seijen, and Eric Eaton. Modular lifelong reinforcement learning via neural composition. In *International Conference on Learning Representations*, 2022b.

Sarthak Mittal, Alex Lamb, Anirudh Goyal, Vikram Voleti, Murray Shanahan, Guillaume Lajoie, Michael Mozer, and Yoshua Bengio. Learning to combine top-down and bottom-up signals in recurrent neural networks with attention over modules. In *Proceedings of the International Conference on Machine Learning (ICML)*, 2020.

Abby O'Neill, Abdul Rehman, Abhiram Maddukuri, Abhishek Gupta, Abhishek Padalkar, Abraham Lee, Acorn Pooley, Agrim Gupta, Ajay Mandlekar, Ajinkya Jain, Albert Tung, Alex Bewley, Alex Herzog, Alex Irpan, Alexander Khazatsky, Anant Rai, Anchit Gupta, Andrew Wang, Anikait Singh, Animesh Garg, Aniruddha Kembhavi, Annie Xie, Anthony Brohan, Antonin Raffin, Archit Sharma, Arefeh Yavary, Arhan Jain, Ashwin Balakrishna, Ayzaan Wahid, Ben Burgess-Limerick, Beomjoon Kim, Bernhard Schölkopf, Blake Wulfe, Brian Ichter, Cewu Lu, Charles Xu, Charlotte Le, Chelsea Finn, Chen Wang, Chenfeng Xu, Cheng Chi, Chenguang Huang, Christine Chan, Christopher Agia, Chuer Pan, Chuyuan Fu, Coline Devin, Danfei Xu, Daniel Morton, Danny Driess, Daphne Chen, Deepak Pathak, Dhruv Shah, Dieter Büchler, Dinesh Jayaraman, Dmitry Kalashnikov, Dorsa Sadigh, Edward Johns, Ethan Foster, Fangchen Liu, Federico Ceola, Fei Xia, Feiyu Zhao, Freek Stulp, Gaoyue Zhou, Gaurav S. Sukhatme, Gautam Salhotra, Ge Yan, Gilbert Feng, Giulio Schiavi, Glen Berseth, Gregory Kahn, Guanzhi Wang, Hao Su, Hao-Shu Fang, Haochen Shi, Henghui Bao, Heni Ben Amor, Henrik I Christensen, Hiroki Furuta, Homer Walke, Hongjie Fang, Huy Ha, Igor Mordatch, Ilija Radosavovic, Isabel Leal, Jacky Liang, Jad Abou-Chakra, Jaehyung Kim, Jaimyn Drake, Jan Peters, Jan Schneider, Jasmine Hsu, Jeannette Bohg, Jeffrey Bingham, Jeffrey Wu, Jensen Gao, Jiaheng Hu, Jiajun Wu, Jialin Wu, Jiankai Sun, Jianlan Luo, Jiayuan Gu, Jie Tan, Jihoon Oh, Jimmy Wu, Jingpei Lu, Jingyun Yang, Jitendra Malik, João Silvério, Joey Hejna, Jonathan Booher, Jonathan Tompson, Jonathan Yang, Jordi Salvador, Joseph J. Lim, Junhyek Han, Kaiyuan Wang, Kanishka Rao, Karl Pertsch, Karol Hausman, Keegan Go, Keerthana Gopalakrishnan, Ken Goldberg, Kendra Byrne, Kenneth Oslund, Kento Kawaharazuka, Kevin Black, Kevin Lin, Kevin Zhang, Kiana Ehsani, Kiran Lekkala, Kirsty Ellis, Krishan Rana, Krishnan Srinivasan, Kuan Fang, Kunal Pratap Singh, Kuo-Hao Zeng, Kyle Hatch, Kyle Hsu, Laurent Itti, Lawrence Yunliang Chen, Lerrel Pinto, Li Fei-Fei, Liam Tan, Linxi Jim Fan, Lionel Ott, Lisa Lee, Luca Wehs, Magnum Chen, Marion Lepert, Marius Memmel, Masayoshi Tomizuka, Masha Itkina, Mateo Guaman Castro, Max Spero, Maximilian Du, Michael Ahn, Michael C. Yip, Mingtong Zhang, Mingyu Ding, Minho Heo, Mohan Kumar Srirama, Mohit Sharma, Moo Jin Kim, Naoaki Kanazawa, Nicklas Hansen, Nicolas Heess, Nikhil J Joshi, Niko Suenderhauf, Ning Liu, Norman Di Palo, Nur Muhammad Mahi Shafullah, Oier Mees, Oliver Kroemer, Osbert Bastani, Pannag R Sanketi, Patrick Tree Miller, Patrick Yin, Paul Wohlhart, Peng Xu, Peter David Fagan, Peter Mitrano, Pierre Sermanet, Pieter Abbeel, Priya Sundaresan, Qiuyu Chen, Quan Vuong, Rafael Rafailov, Ran Tian, Ria Doshi, Roberto Martín-Martín, Rohan Baijal, Rosario Scalise, Rose Hendrix, Roy Lin, Runjia Qian, Ruohan Zhang, Russell Mendonca, Rutav Shah, Ryan Hoque, Ryan Julian, Samuel Bustamante, Sean Kirmani, Sergey Levine, Shan Lin, Sherry Moore, Shikhar Bahl, Shivin Dass, Shubham Sonawani, Shuran Song, Sichun Xu, Siddhant Haldar, Siddharth Karamcheti, Simeon Adebola, Simon Guist, Soroush Nasiriany, Stefan Schaal, Stefan Welker, Stephen Tian, Subramanian Ramamoorthy, Sudeep Dasari, Suneel Belkhale, Sungjae Park, Suraj Nair, Suvir Mirchandani, Takayuki Osa, Tanmay Gupta, Tatsuya Harada, Tatsuya Matsushima, Ted Xiao, Thomas Kollar, Tianhe Yu, Tianli Ding, Todor Davchev, Tony Z. Zhao, Travis Armstrong, Trevor Darrell, Trinity Chung, Vidhi Jain, Vincent Vanhoucke, Wei Zhan, Wenxuan Zhou, Wolfram Burgard, Xi Chen, Xiaolong Wang, Xinghao Zhu, Xinyang Geng, Xiyuan Liu, Xu Liangwei, Xuanlin Li, Yao Lu, Yecheng Jason Ma, Yejin Kim, Yevgen Chebotar, Yifan Zhou, Yifeng Zhu, Yilin Wu, Ying Xu, Yixuan Wang, Yonatan Bisk, Yoonyoung Cho, Youngwoon Lee, Yuchen Cui, Yue Cao, Yueh-Hua Wu, Yujin Tang, Yuke Zhu, Yunchu Zhang, Yunfan Jiang, Yunshuang Li, Yunzhu Li, Yusuke Iwasawa, Yutaka Matsuo, Zehan Ma, Zhuo Xu, Zichen Jeff Cui, Zichen Zhang, and Zipeng Lin. Open x-embodiment: Robotic learning datasets and rt-x models :

---

Open x-embodiment collaboration0. In *2024 IEEE International Conference on Robotics and Automation (ICRA)*, pp. 6892–6903, 2024. doi: 10.1109/ICRA57147.2024.10611477.

William Peebles and Saining Xie. Scalable diffusion models with transformers. In *Proceedings of the IEEE/CVF International Conference on Computer Vision (ICCV)*, 2023.

Han Qi, Changhe Chen, and Heng Yang. Compose by focus: Scene graph-based atomic skills. *arXiv preprint arXiv:2509.16053*, 2025.

John Schulman, Filip Wolski, Prafulla Dhariwal, Alec Radford, and Oleg Klimov. Proximal policy optimization algorithms. *arXiv preprint arXiv:1707.06347*, 2017.

Ilia Shumailov, Zakhar Shumaylov, Yiren Zhao, Nicolas Papernot, Ross J. Anderson, and Yarin Gal. Ai models collapse when trained on recursively generated data. *Nat.*, 631(8022):755–759, July 2024.

Ritvik Singh, Jingzhou Liu, Karl Van Wyk, Yu-Wei Chao, Jean-Francois Lafleche, Florian Shkurti, Nathan Ratliff, and Ankur Handa. Synthetica: Large scale synthetic data generation for robot perception. *arXiv preprint*, 2024.

Ashish Vaswani, Noam Shazeer, Niki Parmar, Jakob Uszkoreit, Llion Jones, Aidan N Gomez, Łukasz Kaiser, and Illia Polosukhin. Attention is all you need. In *Advances in Neural Information Processing Systems*, 2017.

Claas A Voelcker, Marcel Hussen, Eric Eaton, Amir massoud Farahmand, and Igor Gilitschenski. MAD-TD: Model-augmented data stabilizes high update ratio RL. In *The Thirteenth International Conference on Learning Representations*, 2025.

Homer Walke, Kevin Black, Abraham Lee, Moo Jin Kim, Max Du, Chongyi Zheng, Tony Zhao, Philippe Hansen-Estruch, Quan Vuong, Andre He, Vivek Myers, Kuan Fang, Chelsea Finn, and Sergey Levine. Bridgedata v2: A dataset for robot learning at scale. In *Conference on Robot Learning (CoRL)*, 2023.

Renhao Wang, Jiayuan Mao, Joy Hsu, Hang Zhao, Jiajun Wu, and Yang Gao. Programmatically grounded, compositionally generalizable robotic manipulation. In *Proceedings of the International Conference on Learning Representations (ICLR)*, 2023.

Yufei Wang, Zhou Xian, Feng Chen, Tsun-Hsuan Wang, Yian Wang, Katerina Fragkiadaki, Zackory Erickson, David Held, and Chuang Gan. Robogen: Towards unleashing infinite data for automated robot learning via generative simulation. In *International Conference on Machine Learning*, 2024.

Danfei Xu, Suraj Nair, Yuke Zhu, Julian Gao, Animesh Garg, Li Fei-Fei, and Silvio Savarese. Neural task programming: Learning to generalize across hierarchical tasks. In *Proceedings of the IEEE International Conference on Robotics and Automation (ICRA)*, 2018.

Ruihan Yang, Huazhe Xu, Yi Wu, and Xiaolong Wang. Multi-task reinforcement learning with soft modularization. In *Advances in Neural Information Processing Systems (NeurIPS)*, 2020.

Alan Yu, Ge Yang, Ran Choi, Yajvan Ravan, John Leonard, and Phillip Isola. Learning visual parkour from generated images. In *Conference on Robot Learning*, 2024.

Justin Yu, Max Letian Fu, Huang Huang, Karim El-Refai, Rares Andrei Ambrus, Richard Cheng, Muhammad Zubair Irshad, and Ken Goldberg. Real2render2real: Scaling robot data without dynamics simulation or robot hardware. *arXiv preprint arXiv:2505.09601v1*, 2025.

Tianhe Yu, Ted Xiao, Austin Stone, Jonathan Tompson, Anthony Brohan, Su Wang, Jaspia Singh, Clayton Tan, Dee M, Jodilyn Peralta, Brian Ichter, Karol Hausman, and Fei Xia. Scaling robot learning with semantically imagined experience. In *arXiv preprint arXiv:2302.11550*, 2023.

Allan Zhou, Vikash Kumar, Chelsea Finn, and Aravind Rajeswaran. Policy architectures for compositional generalization in control. *Reinforcement Learning Journal*, 5:2264–2283, 2025.

---

Siyuan Zhou, Yilun Du, Jiaben Chen, Yandong Li, Dit-Yan Yeung, and Chuang Gan. RoboDreamer: Learning compositional world models for robot imagination. In Ruslan Salakhutdinov, Zico Kolter, Katherine Heller, Adrian Weller, Nuria Oliver, Jonathan Scarlett, and Felix Berkenkamp (eds.), *Proceedings of the 41st International Conference on Machine Learning*, volume 235 of *Proceedings of Machine Learning Research*, pp. 61885–61896. PMLR, 21–27 Jul 2024.

## A Regime to Study Compositionality in CompoSuite

When sufficient expert data is available, standard feed-forward policies trained with behavioral cloning on the CompoSuite datasets achieve non-trivial zero-shot generalization (Hussing et al., 2024). However, this assumes access to expert trajectories for hundreds of tasks, which is unrealistic in many robotics applications. As data becomes sparser, exploiting the compositional structure of the tasks becomes more relevant. Here, we verify that the data regime of 14 training tasks from Sections 4.2–4.4 is appropriate for studying compositionality. Using all 10 task-lists from the experimental setup suggested by Hussing et al. (2024), we construct subsets of training tasks using the first  $N$  tasks from each list, where  $N \in \{56, 98, 140, 182, 224\}$ , keeping the set of 32 test tasks fixed across values of  $N$ . We then train the SynthER-based architecture introduced in section 4.1 on each subset of training tasks. We generate one million transitions for each test task and train a per-task TD3-BC agent on the generated data. We measure the difference in accumulated return over a set of evaluation trajectories relative to a TD3-BC agent trained on real data. We expect that when the amount of available training data becomes small, the TD3-BC performance should decrease as the generated data quality on out-of-distribution tasks decreases. We report the results in Figure 9.

The results show that when more than 182 tasks are available for training the diffusion models, the mean gap to the ground-truth policy performance is less than 15%. While even the diffusion model trained on 98 tasks achieves high zero-shot generalization, we see a downward trend below this point. As expected, when we move to 56 tasks (roughly 20% of the tasks) the performance gap increases drastically, and the model is unable to zero-shot generalize meaningfully. This is a similar data regime to the 14/64 tasks we used to show the ability of our compositional DiT to learn the underlying graph compositional structure.

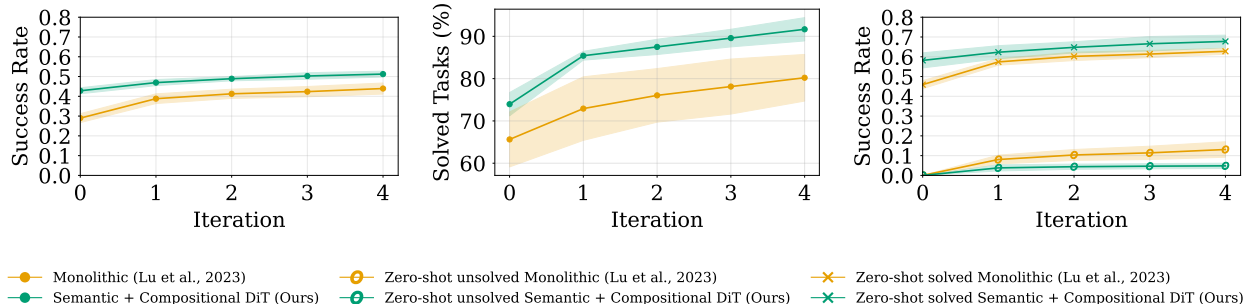


Figure 10: Performance of the monolithic SynthER-based diffusion architecture and the semantic compositional diffusion transformer over iterations of the self-improvement procedure in the 56/256-task training regime. (Left) Zero-shot best success rate achieved so far. RL agents trained on synthetic data from the semantic compositional diffusion architecture consistently achieve higher success rates than agents trained on data from the monolithic SynthER-style diffusion architecture. (Middle) Number of tasks solved at least once across iterations. The semantic compositional diffusion transformer enables policies to solve a substantially larger fraction of tasks at least once compared to the monolithic baseline. (Right) Zero-shot best success rate achieved so far, separated by initial task difficulty. Tasks are partitioned into those that exhibit non-zero success at iteration 0 and those that were entirely unsolved. The semantic compositional architecture particularly improves performance on tasks for which some initial success is already obtained. Shaded regions indicate standard error over 3 diffusion seeds.

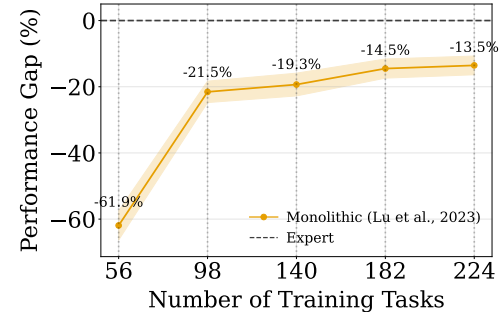


Figure 9: Return difference between RL policies trained on data generated by the monolithic architecture and policies trained on ground-truth data over varying number of training tasks. As the number of training tasks approaches 56 ( $\sim 20\%$ ), there is steep increase in the performance gap indicating the sub-optimality of generated data from the diffusion model.

Figure 9: Return difference between RL policies trained on data generated by the monolithic architecture and policies trained on ground-truth data over varying number of training tasks. As the number of training tasks approaches 56 ( $\sim 20\%$ ), there is steep increase in the performance gap indicating the sub-optimality of generated data from the diffusion model.

---

To further validate that this regime exhibits behavior consistent with our IIWA-only setting, we repeat the iterative data generation procedure in the 56/256-task regime and directly compare the monolithic SynthER-style diffusion model with our semantic compositional diffusion transformer architecture. Figure 10 reports the evolution of zero-shot success rates and solved-task coverage over iterations of Algorithm 1.

We observe similar trends to those in Figure 6: both architectures benefit from iterative self-improvement, while policies trained on data generated by the semantic compositional model consistently achieve higher zero-shot success rates and solve a larger fraction of tasks at least once across iterations. Notably, the performance gap between the monolithic and semantic compositional model is slightly reduced in the 56/256 setting. This is expected, as increasing the number of compositional axes while preserving a comparable training-task ratio exposes the monolithic model to a broader set of task combinations, partially alleviating the severity of the generalization challenge. Importantly, the compositional model continues to exhibit a clear advantage, indicating that the benefits of exploiting task structure persist beyond the IIWA-only setting.

Finally, separating tasks by initial difficulty reveals a similar asymmetry to that observed in the main experiments. While the semantic compositional model improves in both regimes, it exhibits substantially larger gains on tasks that achieve non-zero success at iteration 0, with more gradual improvements on initially unsolved tasks. This behavior is consistent with the interpretation that the model refines factor-specific encoder-decoder representations using self-generated data. Overall, these results support the conclusion that the 14/64 IIWA-only setting constitutes a particularly challenging low-data regime, and that the qualitative self-improvement dynamics of the semantic compositional diffusion model are stable as the number of compositional task axes increases.

## B Additional Experimental Details

This section provides details of the experimental setting used to obtain all results in the paper.

**Computational Requirements** All experiments were conducted on a SLURM-managed GPU cluster equipped with NVIDIA RTX 2080 Ti, RTX 3090, RTX A10, RTX A40, RTX A6000, and L40 GPUs. Training jobs were distributed across these node types, and all model and batch-size configurations were selected to run reliably within the memory constraints of this mixed hardware environment.

### B.1 Compositional Data Generation

#### B.1.1 Diffusion Model Training

We train diffusion models on transition tuples  $(s, a, r, s', d)$  with total dimension 164: a 77-dimensional state, an 8-dimensional action, a scalar reward, a 77-dimensional next state, and a binary terminal indicator. All continuous dimensions are standardized (zero mean, unit variance) using statistics computed from the pooled dataset of all training tasks. The terminal indicator remains unnormalized and is discretized with a threshold of 0.5. All model variants use the same Elucidated Diffusion schedule; differences arise only from the denoiser architecture and a small number of optimization hyperparameters.

During training, noise levels are sampled from a log-normal distribution with mean  $P_{\text{mean}} = -1.2$  and standard deviation  $P_{\text{std}} = 1.2$ . The loss weighting function uses  $\sigma_{\text{data}} = 1.0$ , and the noise schedule spans  $\sigma \in [0.002, 80]$  with curvature parameter  $\rho = 7$ . Tasks are encoded as 16-dimensional binary indicator vectors, as illustrated in Figure 3, and these task indicators condition the denoiser during both training and generation. The complete set of architectural and optimization hyperparameters for the **Monolithic** baseline (Lu et al., 2023) and our **Semantic + Compositional DiT** (S+C DiT) model is listed in Table 1.

#### B.1.2 Data Generation

After each diffusion model is trained, we generate synthetic transition datasets for individual tasks using the EMA (Exponential Moving Average) version of the model. Each task is specified as a 4-tuple (Robot, Object, Obstacle, Objective) and encoded using the same 16-dimensional task indicator from Figure 3. The Monolithic and S+C DiT pipelines use identical sampling configurations, except for the generator

---

Table 1: Diffusion model hyperparameters.

COMPONENT	MONOLITHIC (Lu et al., 2023)	S+C DiT (Ours)
Architecture	6-layer MLP, width 2048	8-layer DiT, hidden size 416, 8 heads (patch size 15 in standard DiT ablation)
Network capacity	25.88M parameters	26.22M parameters
Batch size	1024	1024
Learning rate	$3 \times 10^{-4}$	$1 \times 10^{-4}$
Weight decay	0.0	0.01
Optimizer	AdamW	AdamW
LR scheduler	Cosine	Cosine
Training steps	100,000	100,000

Table 2: Synthetic data generation hyperparameters.

COMPONENT	MONOLITHIC (Lu et al., 2023)	S+C DiT (Ours)
Generated samples per task	1,000,000	1,000,000
Sampling steps	128	128
Noise perturbation strength	80	80
Minimum noise level for perturbation	0.05	0.05
Maximum noise level for perturbation	50	50
Relative perturbation noise scale	1.003	1.003
Generator batch size	100,000	25,000
Batches per task	10	40

batch size, which is reduced for S+C DiT to satisfy GPU memory constraints. The hyperparameters used for synthetic data generation are summarized in Table 2.

### B.1.3 Policy Training

We train TD3-BC policies (Fujimoto & Gu, 2021) on the synthetic transition datasets generated for each task. The same TD3-BC configuration is used across all experiments, including both the monolithic and S+C DiT pipelines and all iterations. The only exception is the compositional RL baselines, which use different compositional policy architectures that are described in Appendix B.2. All policies are trained offline on synthetic data and are then evaluated online in the corresponding CompoSuite environment.

For all test tasks, we train policies using five random seeds and report the mean success rate. States are normalized using the mean and standard deviation computed from each task’s synthetic training dataset. The complete set of TD3-BC hyperparameters used in all experiments is provided in Table 3.

### B.1.4 Iterative Bootstrapping

The iterative bootstrapping procedure follows Algorithm 1. We initialize the success threshold at  $\tau_0 = 0.8$ . If no new tasks satisfy this threshold for one iteration ( $C = 1$ ), the threshold is automatically reduced by  $\Delta_\tau = 0.1$ , with a lower bound of  $\tau_{\min} = 0.5$ . The IIWA-only task list used for this experiment is described in Appendix B.3. The complete set of hyperparameters for this procedure is reported in Table 4.

## B.2 Compositional RL Baselines

We compare against two compositional RL baselines that train multitask TD3-BC policies on expert demonstrations from the same 14 training tasks used for diffusion training. Their train/test split matches the

---

Table 3: TD3-BC offline RL training hyperparameters.

COMPONENT	VALUE
Algorithm	TD3-BC
Actor network	MLP with 2 hidden layers of width 256
Critic networks	MLP with 2 hidden layers of width 256
Learning rate (actor, critics)	$3 \times 10^{-4}$
Optimizer	Adam
Batch size	1024
Training steps	50,000
Discount factor ( $\gamma$ )	0.99
Target network update ( $\tau$ )	0.005
Regularization coefficient ( $\alpha$ )	2.5
Policy noise	0.2
Noise clip	0.5
Policy update frequency	2
Evaluation frequency	5,000 steps
Evaluation episodes	10
State normalization	Yes
Reward normalization	No
Training seeds	0–4

Table 4: Compositional iterative bootstrapping hyperparameters.

COMPONENT	VALUE
Initial success threshold ( $\tau_0$ )	0.8
Minimum threshold ( $\tau_{\min}$ )	0.5
Threshold reduction amount ( $\Delta_\tau$ )	0.1
Patience ( $C$ )	1 iteration
Training tasks ( $ \mathcal{T}_{\text{train}} $ )	56 of 256 tasks, or 14 of 64 IIWA-only tasks
Diffusion seeds	0–2

diffusion setup to allow a fair zero-shot generalization comparison. The list of training and test tasks is described in Appendix B.3. All baselines are evaluated on the corresponding 32 held-out test tasks using 15 random seeds. Both baselines follow the TD3-BC configuration in Table 3, but differ in three ways: (1) they train on a multitask dataset that combines demonstrations from all 14 training tasks, (2) they employ compositional policy architectures, and (3) their batch sizes are scaled with the number of training tasks (i.e., a multiple of the number of tasks), following the strategy used in Mendez et al. (2022a).

The **Hardcoded Compositional RL** (HC RL) baseline uses the modular architecture of Mendez et al. (2022a) with component-specific networks for each task element. The hardcoded architecture follows a hierarchical graph structure with the ordering Obstacle → Object → Subtask → Robot. Hidden layer sizes are (32) for Obstacle, (32, 32) for Object, (64, 64, 64) for Subtask, and (64, 64, 64) for Robot.

The **Semantic Compositional RL** (S+C RL) baseline uses a transformer with semantic tokens corresponding to the object, obstacle, goal, and robot. Compositional encoders produce token embeddings, and task conditioning is applied using Adaptive Layer Normalization (AdaLN). The transformer uses hidden size 72, depth 1, 4 attention heads, MLP ratio 1.20, and no dropout. For this baseline, the batch size is further reduced by one half compared to Mendez et al. (2022a) to satisfy GPU memory constraints.

The full set of hyperparameters is listed in Table 5.

---

Table 5: Compositional RL baseline hyperparameters for multitask TD3-BC training.

COMPONENT	HC RL (Mendez et al., 2022a)	S+C RL (Ours)
Algorithm	TD3-BC	TD3-BC
Training tasks	14	14
Test tasks	32	32
State dimension	93 (with task IDs)	93 (with task IDs)
Action dimension	8	8
Actor architecture	Hardcoded compositional MLP	Semantic compositional transformer
Actor output dimension	8	8
Critic architecture	Hardcoded compositional MLP (state+action)	Semantic compositional transformer (state+action)
Critic output dimension	1	1
Compositional module sizes	(32), (32, 32), (64, 64, 64), (64, 64, 64)	–
Compositional hierarchy	Obstacle → Object → Subtask → Robot	–
Transformer hidden size	–	72
Transformer depth	–	1
Transformer heads	–	4
Transformer MLP ratio	–	1.20
Policy network capacity	107.94K parameters	106.29K parameters
Learning rate	$3 \times 10^{-4}$	$3 \times 10^{-4}$
Optimizer	Adam	Adam
Batch size	3584 (14 tasks $\times$ 256)	1792 (14 tasks $\times$ 128)
Training steps	50,000	50,000
Discount factor ( $\gamma$ )	0.99	0.99
Target network update ( $\tau$ )	0.005	0.005
Regularization coefficient ( $\alpha$ )	2.5	2.5
Policy noise	0.2	0.2
Noise clip	0.5	0.5
Policy update frequency	2	2
Evaluation frequency	5,000 steps	5,000 steps
Evaluation episodes	10 per test task	10 per test task
State normalization	Yes	Yes
Reward normalization	No	No
Training seeds	0–14	0–14

### B.3 Task List

For the results in Appendix A, we use the ten task lists released by Hussen et al. (2024). For the IIWA-only experiments in Section 4, we construct a train/test split over the full IIWA task space, defined by all combinations of the IIWA robot with:

- **Object**: Box, Dumbbell, Hollowbox, Plate,
- **Obstacle**: GoalWall, None, ObjectDoor, ObjectWall,
- **Objective**: PickPlace, Push, Shelf, Trashcan.

This yields  $4 \times 4 \times 4 = 64$  tasks. We generate a random split using seed 0, producing 32 training and 32 test tasks with no overlap. We use the first 14 training tasks for all diffusion and multitask policy experiments, and evaluate on all 32 held-out test tasks. Table 6 lists the tasks, and Figures 11 and 12 visualize the split.

Table 6: Training and test tasks used for IIWA-only experiments.

Training Tasks (14)	Test Tasks (32)
1. IIWA, Box, ObjectDoor, Trashcan	1. IIWA, Dumbbell, GoalWall, Shelf
2. IIWA, Hollowbox, ObjectDoor, PickPlace	2. IIWA, Box, None, PickPlace
3. IIWA, Dumbbell, ObjectDoor, PickPlace	3. IIWA, Box, GoalWall, Shelf
4. IIWA, Dumbbell, ObjectWall, Push	4. IIWA, Hollowbox, None, PickPlace
5. IIWA, Plate, None, Shelf	5. IIWA, Dumbbell, ObjectDoor, Push
6. IIWA, Box, GoalWall, Trashcan	6. IIWA, Box, None, Shelf
7. IIWA, Plate, ObjectWall, Shelf	7. IIWA, Plate, None, PickPlace
8. IIWA, Hollowbox, GoalWall, Trashcan	8. IIWA, Dumbbell, None, Shelf
9. IIWA, Box, ObjectWall, Shelf	9. IIWA, Dumbbell, ObjectDoor, Shelf
10. IIWA, Box, None, Trashcan	10. IIWA, Hollowbox, GoalWall, PickPlace
11. IIWA, Plate, ObjectWall, PickPlace	11. IIWA, Dumbbell, GoalWall, Trashcan
12. IIWA, Box, GoalWall, PickPlace	12. IIWA, Plate, ObjectDoor, Push
13. IIWA, Box, None, Push	13. IIWA, Plate, ObjectDoor, Shelf
14. IIWA, Box, ObjectDoor, Shelf	14. IIWA, Hollowbox, None, Trashcan
	15. IIWA, Box, ObjectDoor, PickPlace
	16. IIWA, Box, ObjectDoor, Push
	17. IIWA, Hollowbox, None, Shelf
	18. IIWA, Dumbbell, ObjectWall, Shelf
	19. IIWA, Hollowbox, GoalWall, Shelf
	20. IIWA, Box, ObjectWall, Push
	21. IIWA, Hollowbox, ObjectWall, Shelf
	22. IIWA, Hollowbox, None, Push
	23. IIWA, Plate, GoalWall, Shelf
	24. IIWA, Plate, ObjectDoor, PickPlace
	25. IIWA, Plate, GoalWall, Trashcan
	26. IIWA, Dumbbell, GoalWall, PickPlace
	27. IIWA, Hollowbox, ObjectDoor, Trashcan
	28. IIWA, Dumbbell, ObjectWall, Trashcan
	29. IIWA, Plate, None, Push
	30. IIWA, Plate, GoalWall, Push
	31. IIWA, Dumbbell, None, Push
	32. IIWA, Plate, GoalWall, PickPlace

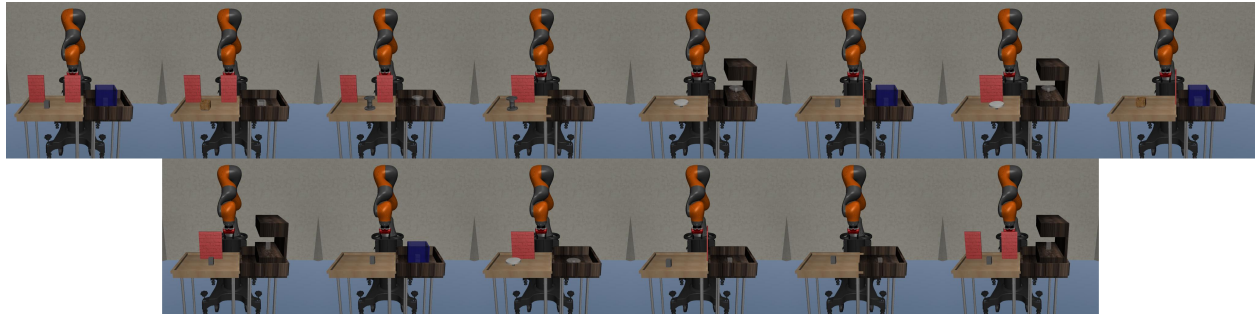


Figure 11: Visualization of the 14 training tasks used in the IIWA-only split. Tasks are shown in numerical order (1–14), arranged left-to-right and top-to-bottom. Each image depicts one unique combination of *Object*, *Obstacle*, and *Objective* paired with the IIWA robot.

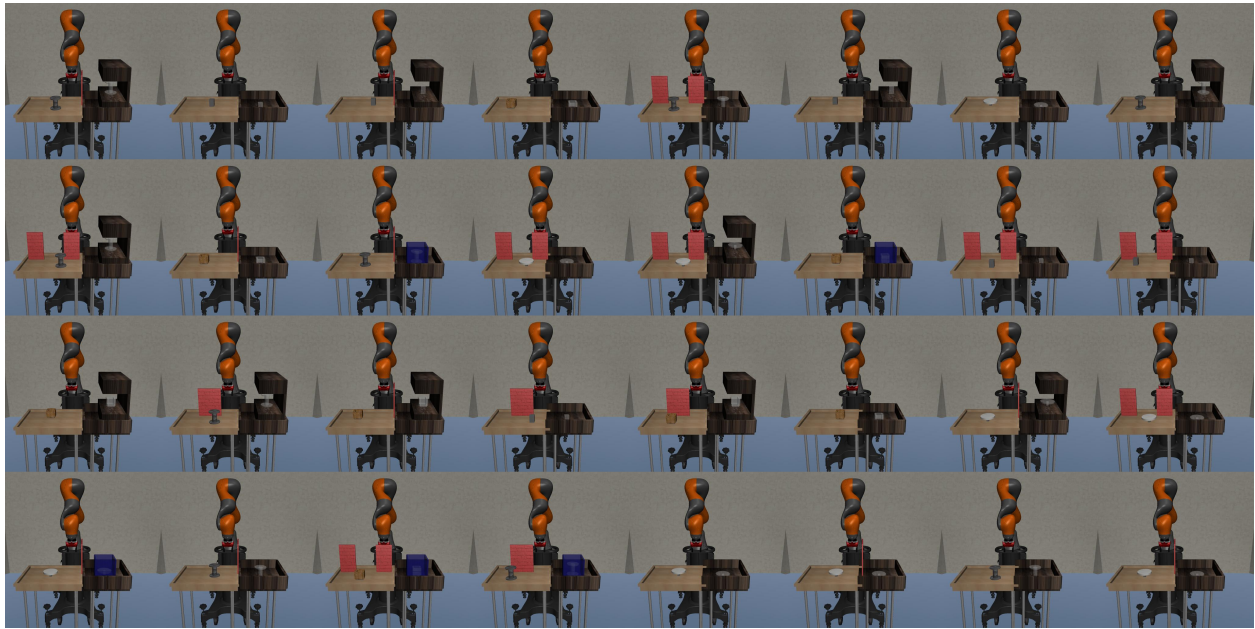


Figure 12: Visualization of the 32 held-out test tasks used for zero-shot evaluation. Tasks are displayed in numerical order (1–32), arranged left-to-right and top-to-bottom. Each image corresponds to a distinct unseen combination of *Object*, *Obstacle*, and *Objective* in the IIWA environment.